Origami metamaterials : design, symmetries, and combinatorics

Dieleman, P.

APPENDIX A

FOLD ANGLES

In this appendix we will derive closed form expressions for the relations between the fold angles of a generic 4-vertex. Expressions in the literature are either in implicit form [48, 76], are for flat foldable vertices only [16, 35, 76], or fail to clearly distinguish between the two possible discrete folding branches [16, 48]. The derivation shown here is originally by Rémi Menaut, and was shortened by Scott Waitukaitis. In addition we will show how the fold angles of a given 4-vertex and its supplement relate to each other.

A Euclidean 4-vertex consists of four rigid plates with sector angles α_i connected by four folds or hinges, where $\sum \alpha_i = 2\pi$ and we assume that all sector angles are unequal and smaller than π (Fig. A.1.A). The non-flat, folded states are characterized by the folding angles ρ_i, defined as the deviation from in-plane alignment between adjacent plates i and $i+1$ (modulo 4). 4-vertices are equivalent to non-intersecting spherical mechanisms, allowing to represent their folded state accordingly (Fig. A.1.B). The fold angles are equal to the angle between the great circles at the point they meet, see ρ_1 in Fig. A.1.B, where we note that ρ_1 here is positive, as it is oriented counterclockwise.

Folding Branches

It was first shown by Huffman that a folded Euclidean 4-vertex will always have one fold whose sign is *unique*, i.e. the angle is opposite in sign from the other folding angles [28, 48, 58]. We call these folds *odd folds*, and these odd folds always straddle a common *odd plate*. A necessary and sufficient condition for the sector angle of the odd plate is the inequality

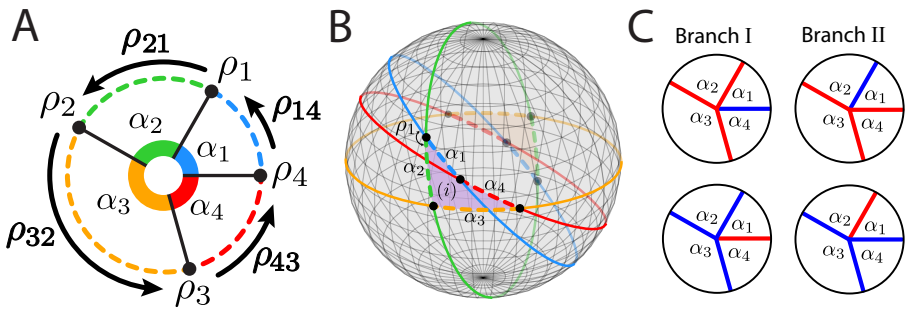

FIGURE A.1: (A) A generic 4-vertex with sector angles α_i, fold angles ρ_i, and fold operators $\boldsymbol{\rho}_{i+1,i}$. (B) An origami vertex (i) can be modeled as a spherical mechanism. Dashed lines trace out the two vertices related by mirror symmetry, whereas the solid lines trace out supplemented vertices. (C) The four possible Mountain-Valley (colored red and blue respectively) arrangements of a generic Euclidean 4-vertex.

$\alpha_i + \alpha_{i+1} < \alpha_{i+2} + \alpha_{i+3}$. A generic 4-vertex always has two odd folds, which straddle a common *odd* plate [28]; we define our vertices such that ρ_4 and ρ_1 are the odd folds, and α_1 is the odd plate. Together with the $\{\rho_i\} \leftrightarrow \{-\rho_i\}$ symmetry, this yields four distinct mountain-valley patterns for a given 4-vertex, shown in Fig. A.1.C. We denote the folding branches where ρ_4 or ρ_1 has the opposite sign by I and II respectively.

Folding Operators

Along a given branch, 4-vertices have one continuous degree of freedom, and the relations between folding angles are anti-symmetric $\rho_i(-\rho_j) = -\rho_i(\rho_j)$ and bijective; we define folding operators $\boldsymbol{\rho}^{\boldsymbol{I,II}}_{i+1,i}$ which map the fold angles adjacent to plate i: $\boldsymbol{\rho}^{\boldsymbol{I,II}}_{i+1,i}(\rho_i) = \rho_{i+1}$, and suppress the index I and II when possible. Here we use the relations between the folding angles to show that the folding operators of a vertex, $\boldsymbol{\rho}_{i+1,i}$ and its supplement, $\boldsymbol{\rho}'_{i+1,i}$ are related as $\boldsymbol{\rho}'_{i+1,i} = -\boldsymbol{\rho}_{i+1,i}$.

We consider a folded state of a 4-vertex, and aim to express all fold angles as function of ρ_4. We schematically represent the arc lengths and dihedral angles of the folded states as seen on the Euclidean sphere by diagrams such as Fig. A.2.B,C. We now consider the arc length λ_{41} between folds ρ_3 and ρ_1, depicted in Fig. A.1.B,C. Using the spherical law of cosines,

we obtain:

$$\cos\lambda_{34} = \cos\alpha_4\cos\alpha_1 - \sin\alpha_4\sin\alpha_1\cos\rho_4\ . \tag{A.1}$$

The arc length λ_{34} is part of two spherical triangles, one with dihedral angles $\pi-\sigma_4$, $\pi-\sigma_1$ and $\pi-\sigma_3$, and the other with $\pi-\tau_1$, $\pi-\tau_2$ and $\pi-\tau_3$. Making use of the shorthand notation,

$$A(a,b,c) \equiv \arccos\left(\frac{\cos a\cos b - \cos c}{\sin a\sin b}\right)\ , \tag{A.2}$$

and repeatedly using the spherical law of cosines, the dihedral angles σ_i and τ_i are,

$$\begin{aligned}
\sigma_1 &= A(\lambda_{34},\alpha_1,\alpha_4) & \tau_1 &= A(\alpha_2,\lambda_{34},\alpha_3)\\
\sigma_3 &= A(\alpha_4,\lambda_{34},\alpha_1) & \tau_2 &= A(\alpha_3,\alpha_2,\lambda_{34})\\
\sigma_4 &= A(\alpha_1,\alpha_4,\lambda_{34}) & \tau_3 &= A(\lambda_{34},\alpha_3,\alpha_2).
\end{aligned}$$

These are all functions or ρ_4 through their dependence on λ_{34}.

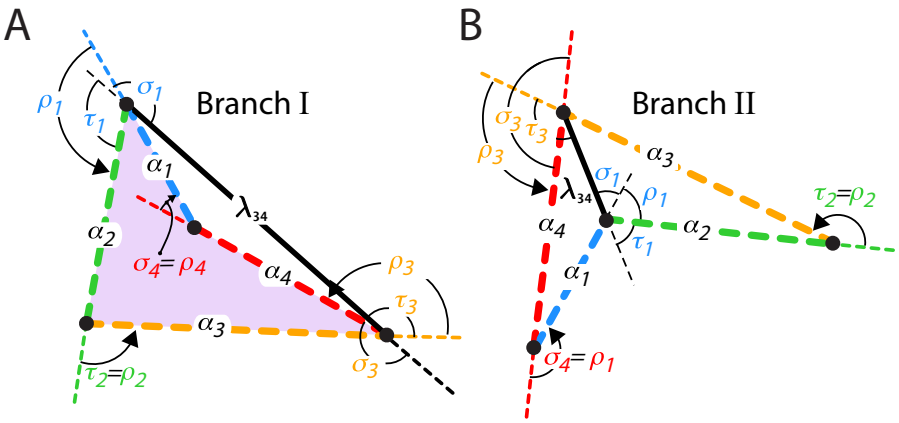

FIGURE A.2: (A) Simplified diagram of a 4-vertex (i) folded in Branch I, as in Fig. A.1.B. (B) Simplified diagram of a 4-vertex folded in Branch II.

We obtain the folding angles from σ_i and τ_i; taking care regarding the relative signs of the fold angles on each branch, the exact equations for

$\rho_4 > 0$ are,

$$\rho_1^{I/II} = -\pi + \sigma_1 \mp \tau_1, \tag{A.3}$$

$$\rho_2^{I/II} = \mp\tau_2, \tag{A.4}$$

$$\rho_3^{I/II} = -\pi + \sigma_3 \mp \tau_3, \tag{A.5}$$

where the minus sign in $\mp$ corresponds to branches I, and the plus sign in $\mp$ to branch II. Because of reflection symmetry in the flat-state plane, these equations are antisymmetric: $[\rho_i^{I/II}(\rho_4 < 0) = -\rho_i^{I/II}(\rho_4 > 0)]$. Similarly, we can obtain expressions for any fold angle as function of any other fold angle.

The operator $\boldsymbol{\rho_{14}}$ follows directly from Eq. A.3. Using these explicit expressions, we now show that $\boldsymbol{\rho'_{i+1,i}} = -\boldsymbol{\rho}_{i+1,i}$. For the supplemented vertex, we modify the sector angles from α_i to $\alpha'_i = \pi - \alpha_i$. First, note that the expression for $\cos(\lambda_{34})$, Eq. A.1, remains identical under this transformation, making use of the identity $\cos(-x) = \cos(x)$ and $\sin(-x) = -\sin(x)$. Second, note that we can write:

$$\begin{aligned}
\sigma'_1 &= A(\lambda_{34}, \alpha'_1, \alpha'_4), \\
&= \arccos\left(\frac{-\cos\lambda_{34}\cos\alpha_1 + \cos\alpha_4}{\sin\lambda_{34}\sin\alpha_1}\right) \\
&= \pi - A(\lambda_{34}, \alpha_1, \alpha_4), \\
&= \pi - \sigma_1
\end{aligned} \tag{A.6}$$

using the identity: $\arccos(-x) = \pi - \arccos(x)$. Likewise, we have $\tau'_1 = \pi - \tau_1$. We therefore find (dropping the branch notation),

$$\begin{aligned}
\rho'_1 &= -\pi + \sigma'_1 \mp \tau'_1, \\
&= -\pi + (\pi - \sigma_1) \mp (\pi - \tau'_1), \\
&= \pi - \sigma_1 \pm \tau_1, \\
&= -\rho_1 \ .
\end{aligned} \tag{A.7}$$

Hence, $\boldsymbol{\rho'_{14}} = -\boldsymbol{\rho_{14}}$, and we can trivially extend this argument to show that $\boldsymbol{\rho'_{i+1,i}} = -\boldsymbol{\rho_{i+1,i}}$.

APPENDIX B

4-VERTEX AS A SPHERICAL MECHANISM

The operator symmetry $\boldsymbol{\rho'_{ij} = -\rho_{ij}}$ derived in appendix A, can also be derived graphically. As shown before, a 4-vertex can be modeled as a spherical mechanism, which can be represented on the surface of a sphere (Fig. A.1.B). In Fig. B.1.A we schematically represent a 4-vertex (i) in a folded configuration, by using a pseudo-Mercator projection. Extending the arcs of vertex (i), we obtain four directed great circles. The intersection of circle i and $i+1$ –indicated by the black circles– correspond to the hinges of spherical linkage (i), whereas their respective angle corresponds to fold angle ρ_i. We define the fold angles ρ_i as positive when ρ_i turns counterclockwise. The grey circles indicate the antipodal points of the black points of vertex (i). Along each directed circle we name the four arc lengths: α_i, $\bar{\alpha}_i$, $\dot{\alpha}_i$, $\tilde{\alpha}_i$, where $\dot{\alpha}_i = \alpha_i$, $\bar{\alpha}_i = \tilde{\alpha}_i = \pi - \alpha_i$, and $\alpha_i + \bar{\alpha}_i + \dot{\alpha}_i + \tilde{\alpha}_i = 2\pi$ (also see Fig. B.1.A). Furthermore, any pair of great circles intersects at two locations, and because they are great circles, the angles around an intersection point are identical in magnitude to the angles around its antipodal point.

We first show that we can derive the relationship between the fold angles (and fold operators) of the four related vertices (i), (ii), (iii) and (iv) of Fig. 2.2. Our goal is to relate the fold angles of vertices (ii), (iii) and (iv) to the fold angles ρ_i of vertex (i) – shaded pink in Fig. B.1.A. First, vertex (ii) –shaded orange in Fig. B.1.A– can be found by connecting the four antipodal (grey) nodes, which consists of arc lengths $\dot{\alpha}_i$. When we

consider the fold angles of this vertex (running clockwise), we see that they are all oppositely oriented with respect to those of vertex (i), and therefore each pick up a minus sign. Thus, if a vertex can be in a configuration with folding angles $\{\rho_i\}$, it can also be in a configuration with folding angles $\{-\rho_i\}$, consistent with $\rho_j(-\rho_i) = -\rho_j(\rho_i)$

Second, we consider vertex (iii), which is shaded purple in Fig. B.1.B. This vertex consists of arc lengths: $\tilde{\alpha}_1, \bar{\alpha}_2, \tilde{\alpha}_3, \bar{\alpha}_4$, running clockwise. We see that in this case, only the fold angle around the antipodal (gray) nodes are reversed. The same holds true for vertex (iv) $(\bar{\alpha}_1, \tilde{\alpha}_2, \bar{\alpha}_3, \tilde{\alpha}_4)$, which is shaded orange in Fig. B.1.B. As the resultant fold angles are alternating in sign for both vertex (iii) and (iv), and we find: $\rho_{i+1}(\rho_i) = -\rho_{i+1}(\rho_i)$, or $\boldsymbol{\rho'_{ij} = -\rho_{ij}}$, using the operator notation. We finally note that vertex (i) in Fig. B.1.A depicts a vertex folded on branch I, where ρ_4 is opposite to the three other folds, but the relations above also hold on branch II (where ρ_1 is opposite in sign).

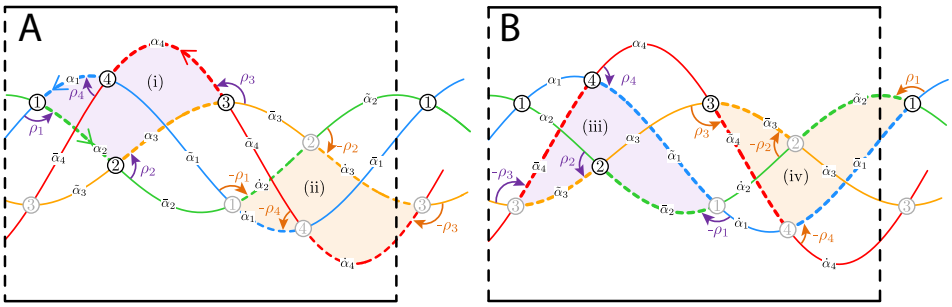

FIGURE B.1: (A) Simplified Mercator projection of a vertex (i) as shown in Fig. A.1, and its mirror image on the other side of the sphere (ii). (B) Simplified Mercator projection of two the two supplemented vertices, (iii) and (iv). Dashed line indicates periodic boundary. For details see text.

Besides the related Euclidean vertices (i)-(iv) and their representative spherical mechanisms (also termed 'folding linkages' [77]), there are an additional 12 related spherical mechanisms [78, 79]. All of these represent non-Euclidean vertices. Some of these mechanisms however, are self-intersecting, meaning they can not be converted into a 4-vertex as the plates would intersect. To study these additional spherical mechanisms in detail, we use the same pseudo-Mercator map as in Fig. B.1, in Fig. B.2. On this map we express all 16 arc lengths (α_i, $\bar{\alpha}_i$, $\dot{\alpha}_i$, $\tilde{\alpha}_i$), as well as the

angles around each node (ρ_i and ρ'_i) in terms of the arc lengths and angles of the original counterclockwise oriented vertex (i), which is depicted by the dashed line.

An example of one the 12 non-Euclidean spherical mechanisms is shown in light-blue in Fig. B.2, which we denote as $\tilde{\alpha}_1\dot{\alpha}_2\bar{\alpha}_3\alpha_4$. When we consider the magnitude of the angles between consecutive links of this mechanism, we find that they are: ρ'_1, ρ'_2, ρ'_3, ρ'_4. The signs of these angles can be found by comparing the orientation of these angles to those of the original vertex (vertex (i) in Fig. B.1.A), where the orientation of the mechanism itself is set by the colors of the segments (blue $\rightarrow$ green $\rightarrow$ yellow $\rightarrow$ red). In this case, the orientation of the angles in the mechanism $\tilde{\alpha}_1\dot{\alpha}_2\bar{\alpha}_3\alpha_4$ are respectively: counterclockwise, counterclockwise, clockwise, and counterclockwise. When comparing this to vertex (i), we see that both ρ'_3 and ρ'_4 are oppositely oriented, which is why they obtain a minus sign. The folding angles of this mechanism are therefore ρ'_1, ρ'_2, $-\rho'_3$, $-\rho'_4$. An example of a self-intersecting non-Euclidean mechanism is colored green in Fig. B.2. This mechanism is denoted as $\bar{\alpha}_1\tilde{\alpha}_2\dot{\alpha}_3\dot{\alpha}_4$. Comparison of the angles of this mechanism to those of vertex (i) yields: ρ_1, ρ'_2, $-\rho_3$, ρ'_4.

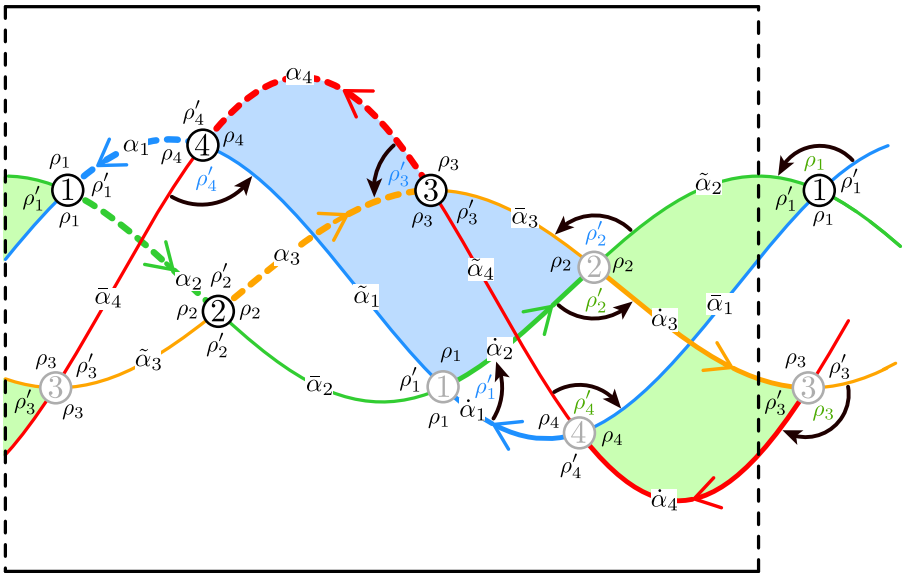

FIGURE B.2: Simplified mercator projection of the flat vertex shown in Fig. A.1 (dashed lines), folded on branch I. Dashed lines indicate periodic boundary.

In Table B.1 we list all 16 spherical mechanisms and their respective arc lengths (β_i), and fold angles (θ_i), expressed in terms of the arc lengths and fold angles of the vertex $\alpha_1\alpha_2\alpha_3\alpha_4$. Although the fold angles derived here are derived from Fig. B.2, which depicts a spherical mechanism on branch I (where the sign of ρ_4 on vertex $\alpha_1\alpha_2\alpha_3\alpha_4$ is opposite to the other three), we note that the expressions are valid for branch II as well (where the sign of ρ_1 on vertex $\alpha_1\alpha_2\alpha_3\alpha_4$ is opposite to the other three). In addition to the fold angles θ_i, we also display the sign of θ_i on both branch I and branch II. From the $\bar{\alpha}_1\tilde{\alpha}_2\dot{\alpha}_3\dot{\alpha}_4$ mechanism we know that self intersecting mechanisms have two consecutive positive fold angles, and two consecutive negative fold angles. We therefore see that mechanisms $\alpha_1\alpha_2\tilde{\alpha}_3\bar{\alpha}_4$, $\tilde{\alpha}_1\bar{\alpha}_2\alpha_3\alpha_4$, $\dot{\alpha}_1\dot{\alpha}_2\bar{\alpha}_3\tilde{\alpha}_4$, and $\bar{\alpha}_1\tilde{\alpha}_2\dot{\alpha}_3\dot{\alpha}_4$ are self-intersecting on branch I. On branch II we find that $\alpha_1\tilde{\alpha}_2\bar{\alpha}_3\alpha_4$, $\tilde{\alpha}_1\dot{\alpha}_2\dot{\alpha}_3\bar{\alpha}_4$, $\dot{\alpha}_1\bar{\alpha}_2\tilde{\alpha}_3\dot{\alpha}_4$, and $\bar{\alpha}_1\alpha_2\alpha_3\tilde{\alpha}_4$ are self intersecting. Other than the four Euclidean vertices $\alpha_1\alpha_2\alpha_3\alpha_4$, $\tilde{\alpha}_1\bar{\alpha}_2\tilde{\alpha}_3\bar{\alpha}_4$, $\dot{\alpha}_1\dot{\alpha}_2\dot{\alpha}_3\dot{\alpha}_4$, $\bar{\alpha}_1\tilde{\alpha}_2\bar{\alpha}_3\tilde{\alpha}_4$, this leaves four spherical mechanisms that represent non-Euclidean vertices which can fold from branch I to branch II, these are: $\alpha_1\tilde{\alpha}_2\dot{\alpha}_3\bar{\alpha}_4$, $\tilde{\alpha}_1\dot{\alpha}_2\bar{\alpha}_3\alpha_4$, $\dot{\alpha}_1\bar{\alpha}_2\alpha_3\tilde{\alpha}_4$, $\bar{\alpha}_1\alpha_2\bar{\alpha}_3\dot{\alpha}_4$.

Arc Lengths				Folding Angle				Sign (Branch I)				Sign (Branch II)			
β_1	β_2	β_3	β_4	θ_1	θ_2	θ_3	θ_4	θ_1	θ_2	θ_3	θ_4	θ_1	θ_2	θ_3	θ_4
α_1	α_2	α_3	α_4	ρ_1	ρ_2	ρ_3	ρ_4	$+$	$+$	$+$	$-$	$-$	$+$	$+$	$+$
α_1	$\tilde{\alpha_2}$	$\bar{\alpha_3}$	α_4	$-\rho_1'$	$-\rho_2$	$-\rho_3'$	ρ_4	$-$	$-$	$-$	$-$	$+$	$-$	$-$	$+$
α_1	α_2	$\tilde{\alpha_3}$	$\bar{\alpha_4}$	ρ_1	$-\rho_2'$	$-\rho_3$	$-\rho_4'$	$+$	$-$	$-$	$+$	$-$	$-$	$-$	$-$
α_1	$\tilde{\alpha_2}$	$\dot{\alpha_3}$	$\bar{\alpha_4}$	$-\rho_1'$	ρ_2'	ρ_3'	$-\rho_4'$	$-$	$+$	$+$	$+$	$+$	$+$	$+$	$-$
$\tilde{\alpha_1}$	$\bar{\alpha_2}$	$\tilde{\alpha_3}$	$\bar{\alpha_4}$	$-\rho_1$	ρ_2	$-\rho_3$	ρ_4	$-$	$+$	$-$	$-$	$+$	$+$	$-$	$+$
$\tilde{\alpha_1}$	$\dot{\alpha_2}$	$\dot{\alpha_3}$	$\bar{\alpha_4}$	ρ_1'	$-\rho_2$	ρ_3'	ρ_4	$+$	$-$	$+$	$-$	$-$	$-$	$+$	$+$
$\tilde{\alpha_1}$	$\bar{\alpha_2}$	α_3	α_4	$-\rho_1$	$-\rho_2'$	ρ_3	$-\rho_4'$	$-$	$-$	$+$	$+$	$+$	$-$	$+$	$-$
$\tilde{\alpha_1}$	$\dot{\alpha_2}$	$\bar{\alpha_3}$	α_4	ρ_1'	ρ_2'	$-\rho_3'$	$-\rho_4'$	$+$	$+$	$-$	$+$	$-$	$+$	$-$	$-$
$\dot{\alpha_1}$	$\dot{\alpha_2}$	$\dot{\alpha_3}$	$\dot{\alpha_4}$	$-\rho_1$	$-\rho_2$	$-\rho_3$	$-\rho_4$	$-$	$-$	$-$	$+$	$+$	$-$	$-$	$-$
$\dot{\alpha_1}$	$\bar{\alpha_2}$	$\tilde{\alpha_3}$	$\dot{\alpha_4}$	ρ_1'	ρ_2	ρ_3'	$-\rho_4$	$+$	$+$	$+$	$+$	$-$	$+$	$+$	$-$
$\dot{\alpha_1}$	$\dot{\alpha_2}$	$\bar{\alpha_3}$	$\tilde{\alpha_4}$	$-\rho_1$	ρ_2'	ρ_3	ρ_4'	$-$	$+$	$+$	$-$	$+$	$+$	$+$	$+$
$\dot{\alpha_1}$	$\bar{\alpha_2}$	α_3	$\tilde{\alpha_4}$	ρ_1'	$-\rho_2'$	$-\rho_3'$	ρ_4'	$+$	$-$	$-$	$-$	$-$	$-$	$-$	$+$
$\bar{\alpha_1}$	$\tilde{\alpha_2}$	$\bar{\alpha_3}$	$\tilde{\alpha_4}$	ρ_1	$-\rho_2$	ρ_3	$-\rho_4$	$+$	$-$	$+$	$+$	$-$	$-$	$+$	$-$
$\bar{\alpha_1}$	α_2	α_3	$\tilde{\alpha_4}$	$-\rho_1'$	ρ_2	$-\rho_3'$	$-\rho_4$	$-$	$+$	$-$	$+$	$+$	$+$	$-$	$-$
$\bar{\alpha_1}$	$\tilde{\alpha_2}$	$\dot{\alpha_3}$	$\dot{\alpha_4}$	ρ_1	ρ_2'	$-\rho_3$	ρ_4'	$+$	$+$	$-$	$-$	$-$	$+$	$-$	$+$
$\bar{\alpha_1}$	α_2	$\tilde{\alpha_3}$	$\dot{\alpha_4}$	$-\rho_1'$	$-\rho_2'$	ρ_3'	ρ_4'	$-$	$-$	$+$	$-$	$+$	$-$	$+$	$+$

TABLE B.1: Table listing all 16 spherical mechanisms that can be linked to a generic Euclidean 4-vertex, and their fold angles.

Bibliography

[1] P. Wang-Iverson, R. J. Lang, and M. Yim. *Origami 5: Fifth International Meeting of Origami Science, Mathematics, and Education*. A K Peters/CRC Press, New York, 2011. ISBN 9781439873502. doi:10.1201/b10971.

[2] D. Lister. Some observations on the history of paperfolding in Japan and the West – a development in parallel. In K. Miura, editor, *Origami Science and Art: Proceedings of the Second International Meeting of Origami Science and Scientific Origami*, pages 511–524, Natick, Massachusetts, 1997. A K Peters.

[3] Unknown. *Hiden Senbazuru Orikata ("How to Fold a Thousand Cranes")*. Japan, 1797.

[4] Anonymous. *Aanhangzel van de volmaakte Hollandsche keuken-meid*. chapter: "de Wyze om allerhande Tafel-goed Konstig en cierlyk te vouwen". Steven van Esveldt, Amsterdam, fourth edition, 1754.

[5] (A) Wikipedia. *Hiden Senbazuru Orikata*. https://upload.wikimedia.org/wikipedia/commons/7/71/Hiden_Senbazuru_Orikata-S6-2.jpg. (B) F. J. Haffmans. *Uitvouwbare doopbrief, Duitsland, 1769*. http://haffmansantiek.nl/peetvaderbrief-patenbrief-duitsland-18e-eeuw-doopsel.html. (C) Brabants museum. *Kookboeken uit vroeger tijd*. https://brabant-collectie.blogspot.nl/2014/12/kookboeken-uit-vroeger-tijd.html.

[6] C. Totman. *A history of Japan*. Wiley-Blackwell, 2nd edition edition, 2014. ISBN 9781405123594.

[7] N. Robinson. *The Origami Bible*. Collins & Brown Limited, London, 2004. ISBN 9781581805178.

[8] R.C. Yates. *Geometrical Tools: A Mathematical Sketch and Model Book*. Educational Publishers, St. Louis, Missouri, 1949.

[9] K. Kasahara and T. Takahama. *Origami for the Connoisseur*. Japan Publications, New York, New York, 1987. ISBN 9780870406706.

[10] T. Kawasaki. On high dimensional flat origamis. In H. Huzita, editor, *Proceedings of the First International Meeting of Origami Science and Technology*, pages 131–141. Commune di Ferra and Centro Origami Duffusion, 1989.

[11] T. C. Hull. On the mathematics of flat origamis. *Congressus numerantium*, pages 215–224, 1994.

[12] J. Justin. Towards a mathematical theory of origami. In K. Miura, editor, *Origami Science and Art: Proceedings of the Second International Meeting of Origami and Scientific Origami*, pages 15–29, Natick, Massachusetts, 1997. A K Peters.

[13] T. C. Hull. The combinatorics of flat folds: a survey. In T. C. Hull, editor, *Origami 3: Third International Meeting of Origami Science, Mathematics, and Education*, pages 29–38, Natick, Massachusetts, 2002. A K Peters.

[14] E. D. Demaine and J. O'Rourke. *Geometric Folding Algorithms: Linkages, Origami, Polyhedra*. Cambridge University Press, Cambridge, 2007. doi:10.1017/cbo9780511735172.

[15] J. Ginepro and T. C. Hull. Counting Miura-ori foldings. *J. Integer Seq.*, 17(2):3, 2014.

[16] T. Tachi. Generalization of rigid foldable quadrilateral mesh origami. In A. Domingo Cabo and C. L. Lázaro Fernández, editors, *Symposium of the International Association for Shell and Spatial Structures (IASS): Evolution and Trends in Design, Analysis and Construction of Shell and Spatial Structures*, pages 2287–2294, Valencia, 2009. Editorial Universitat Politècnica de València.

[17] R. J. Lang. Treemaker 4.0: A program for origami design, 1998. URL http://www.langorigami.com/files/articles/TreeMkr40.pdf.

[18] T. Tachi. Origamizing polyhedral surfaces. *IEEE Trans. Vis. Comput. Graph*, 16(2):298–311, 2010. doi:10.1109/tvcg.2009.67.

[19] E. D. Demaine and T. Tachi. Origamizer: A practical algorithm for folding any polyhedron. In B. Aronov and M. J. Kat, editors, *33rd International Symposium on Computational Geometry (SoCG 2017)*, volume 77. Leibniz International Proceedings in Informatics, 2017. doi:10.4230/LIPIcs.SoCG.2017.34.

[20] E. G. Rapp. Sandwich-type structural element, December 6 1960. US Patent 2,963,128.

[21] L. C. Gewiss. Method for forming herringbone configurations for sandwich structures, March 18 1969. US Patent 3,433,692.

[22] K. Miura. Zeta-core sandwich - its concept and realization. *ISAS report, University of Tokyo*, 37(6):137–164, 1972.

[23] A. Lebée. From folds to structures, a review. *Int. J. Space Struct.*, 30(2): 55–74, 2015. doi:10.1260/0266-3511.30.2.55.

[24] E. Baranger, P. Guidault, and C. Cluzel. Generation of physical defects for the prediction of the behavior of folded cores. In *Fourth European Congress on Computational Mechanics (ECCM IV)*, 2010.

[25] E. Baranger, P. Guidault, and C. Cluzel. Numerical modeling of the geometrical defects of an origami-like sandwich core. *Compos. Struct.*, 93(10):2504–2510, 2011. doi:10.1016/j.compstruct.2011.04.011.

[26] M. Schenk and S. D. Guest. Geometry of Miura-folded metamaterials. *Proc. Natl. Acad. Sci.*, 110(9):3276–3281, 2013. doi:10.1073/pnas.1217998110.

[27] J. L. Silverberg, A. A. Evans, L. McLeod, R. C. Hayward, T. C. Hull, C. D. Santangelo, and I. Cohen. Using origami design principles to fold reprogrammable mechanical metamaterials. *Science*, 345(6197): 647–650, 2014. doi:10.1126/science.1252876.

[28] S. Waitukaitis, R. Menaut, B.G. Chen, and M. van Hecke. Origami multistability: From single vertices to metasheets. *Phys. Rev. Lett.*, 114 (5):055503, 2015. doi:10.1103/physrevlett.114.055503.

[29] S. Felton, M. Tolley, E. D. Demaine, D. Rus, and R. J. Wood. A method for building self-folding machines. *Science*, 345(6197):644–646, 2014. doi:10.1126/science.1252610.

[30] A. Firouzeh and J. Paik. Robogami: A fully integrated low-profile robotic origami. *J. Mech. Rob.*, 7(2):021009, 2015. doi:10.1115/1.4029491.

[31] C. D. Onal, M. T. Tolley, R. J. Wood, and D. Rus. Origami-inspired printed robots. *IEEE/ASME Trans. Mechatron.*, 20(5):2214–2221, 2015. doi:10.1109/tmech.2014.2369854.

[32] K. Bertoldi, V. Vitelli, J. Christensen, and M. van Hecke. Flexible mechanical metamaterials. *Nat. Rev. Mater.*, 2(17066), 2017. doi:doi:10.1038/natrevmats.2017.66.

[33] K. Miura. Method of packaging and deployment of large membranes in space. *ISAS report, University of Tokyo*, 618:1–9, 1985.

[34] L. H. Dudte, E. Vouga, T. Tachi, and L. Mahadevan. Programming curvature using origami tessellations. *Nat. Mater.*, 15(5):583–588, 2016. doi:10.1038/nmat4540.

[35] Arthur A. Evans, Jesse L. Silverberg, and Christian D. Santangelo. Lattice mechanics of origami tessellations. *Phys. Rev. E*, 92(1):013205, 2015. doi:10.1103/physreve.92.013205.

[36] M. B. Amar and F. Jia. Anisotropic growth shapes intestinal tissues during embryogenesis. *Proc. Natl. Acad. Sci.*, 110(26):10525–10530, 2013. doi:10.1073/pnas.1217391110.

[37] L. Mahadevan and S. Rica. Self-organized origami. *Science*, 307(5716): 1740, 2005. doi:10.1126/science.1105169.

[38] E. Couturier, S. C. Du Pont, and S. Douady. A global regulation inducing the shape of growing folded leaves. *PLoS ONE*, 4(11):e7968, 2009. doi:10.1371/journal.pone.0007968.

[39] H. Kobayashi, B. Kresling, and J. F. V. Vincent. The geometry of unfolding tree leaves. *Proc. R. Soc. B*, 265(1391):147–154, 1998. doi: 10.1098/rspb.1998.0276.

[40] F. Haas and R. J. Wootton. Two basic mechanisms in insect wing folding. *Proc. R. Soc. B*, 263(1377):1651–1658, 1996. doi:10.1098/rspb.1996.0241.

[41] T. Nojima. Origami modeling of functional structures based on organic patterns. Master's thesis, Dept. of Engineering Science, Graduate School of Kyoto University, 2002.

[42] V. Brunck, F. Lechenault, A. Reid, and M. Adda-Bedia. Elastic theory of origami-based metamaterials. *Phys. Rev. E*, 93(3):033005, 2016. doi:10.1103/physreve.93.033005.

[43] A. E. Shyer, T. Tallinen, N. L. Nerurkar, Z. Wei, E. S. Gil, D. L. Kaplan, C. J. Tabin, and L. Mahadevan. Villification: how the gut gets its villi. *Science*, 342(6155):212–218, 2013. doi:10.1126/science.1238842.

[44] F. Lechenault, B. Thiria, and M. Adda-Bedia. Mechanical response of a creased sheet. *Phys. Rev. Lett.*, 112(24):244301, 2014. doi:10.1103/physrevlett.112.244301.

[45] S. Deboeuf, E. Katzav, A. Boudaoud, D. Bonn, and M. Adda-Bedia. Comparative study of crumpling and folding of thin sheets. *Phys. Rev. Lett.*, 110(10):104301, 2013. doi:10.1103/physrevlett.110.104301.

[46] J. C. Maxwell. L. on the calculation of the equilibrium and stiffness of frames. *The London, Edinburgh, and Dublin Philosophical Magazine and Journal of Science*, 27(182):294–299, 1864. doi: 10.1080/14786446408643668.

[47] C. R. Calladine. Buckminster fuller's "tensegrity" structures and Clerk Maxwell's rules for the construction of stiff frames. *Int. J. Solids Struct.*, 14(2):161–172, 1978. doi:10.1016/0020-7683(78)90052-5.

[48] D. A. Huffman. Curvature and creases: A primer on paper. *IEEE Trans. Comput.*, (10):1010–1019, 1976. doi:10.1109/tc.1976.1674542.

[49] A. Kokotsakis. Über bewegliche polyeder. *Math. Ann.*, 107(1):627–647, 1933. doi:10.1007/bf01448912.

[50] H. Stachel. Flexible polyhedral surfaces with two flat poses. *Symmetry*, 7(2):774–787, 2015. doi:10.3390/sym7020774.

[51] P. T. Barreto. Lines meeting on a surface: The “Mars" paperfolding. In K. Miura, editor, *Origami Science and Art: Proceedings of the Second International Meeting of Origami and Scientific Origami*, pages 343–359, Natick, Massachusetts, 1997. A K Peters.

[52] T. Tachi. *Rigid Foldable Quadrilateral Mesh Origami Crease Pattern*. https://www.flickr.com/photos/tactom/4053859811/. Movie of the 3D-folding motion shown in: https://www.flickr.com/photos/tactom/3725723541/.

[53] E. T. Filipov, T. Tachi, and G. H. Paulino. Origami tubes assembled into stiff, yet reconfigurable structures and metamaterials. *Proc. Natl. Acad. Sci.*, 112(40):12321–12326, 2015. doi:10.1073/pnas.1509465112.

[54] E. T. Filipov, G. H. Paulino, and T. Tachi. Origami tubes with reconfigurable polygonal cross-sections. In *Proc. R. Soc. A*, volume 472, page 20150607. The Royal Society, 2016. doi:10.1098/rspa.2015.0607.

[55] X. Liu, J. M. Gattas, and Y. Chen. One-dof superimposed rigid origami with multiple states. *Sci. Rep.*, 6:36883, 2016. doi:10.1038/srep36883.

[56] K. Song, X. Zhou, S. Zang, H. Wang, and Z. You. Design of rigid-foldable doubly curved origami tessellations based on trapezoidal crease patterns. *Proc. R. Soc. A*, 473(2200):20170016, 2017. doi:10.1098/rspa.2017.0016.

[57] T. A. Evans, R. J. Lang, S.P. Magleby, and L. L. Howell. Rigidly foldable origami gadgets and tessellations. *Roy. Soc. Open Sci.*, 2(9):150067, 2015. doi:10.1098/rsos.150067.

[58] S. Waitukaitis and M. van Hecke. Origami building blocks: Generic and special four-vertices. *Phys. Rev. E*, 93(2):023003, Feb 2016. doi:10.1103/physreve.93.023003.

[59] W. K. Schief, A. I. Bobenko, and T. Hoffmann. On the integrability of infinitesimal and finite deformations of polyhedral surfaces. In *Discrete differential geometry*, pages 67–93. Springer, 2008. doi:10.1007/978-3-7643-8621-4_4.

[60] O. N. Karpenkov. On the flexibility of Kokotsakis meshes. *Geom. Dedicata*, 147(1):15–28, 2010. doi:10.1007/s10711-009-9436-4.

[61] H. Stachel. A kinematic approach to Kokotsakis meshes. *Comput. Aided Geom. Des.*, 27(6):428–437, 2010. doi:10.1016/j.cagd.2010.05.002.

[62] M. B. Pinson, M. Stern, A. Ferrero, C. Alexandra, T. A. Witten, E. Chen, and A. Murugan. Self-folding origami at any energy scale. *Nat. Commun.*, 8:15477, 2017. doi:10.1038/ncomms15477.

[63] T. Tachi. Origamizer. URL `http://origami.c.u-tokyo.ac.jp/~tachi/software/`.

[64] T. Tachi. Geometric considerations for the design of rigid origami structures. In *Proceedings of the International Association for Shell and Spatial Structures (IASS) Symposium*, volume 12, pages 458–460. Shanghai, 2010.

[65] R. J. Lang. *Origami Design Secrets: Mathematical Methods for an Ancient Art*. AK Peters/CRC Press, New York, 2nd edition, 2011.

[66] B. H. Hanna, J. M. Lund, R. J. Lang, S. P. Magleby, and L. L. Howell. Waterbomb base: a symmetric single-vertex bistable origami mechanism. *Smart Mater. Struct.*, 23(9):094009, 2014. doi:10.1088/0964-1726/23/9/094009.

[67] F Lechenault and M Adda-Bedia. Generic bistability in creased conical surfaces. *Phys. Rev. Lett.*, 115(23):235501, 2015. doi:10.1103/PhysRevLett.115.235501.

[68] J. L. Silverberg, J. Na, A. A. Evans, B. Liu, T. C. Hull, C. D. Santangelo, R. J. Lang, R. C. Hayward, and I. Cohen. Origami structures with a critical transition to bistability arising from hidden degrees of freedom. *Nat. Mater.*, 14(4):389–393, 2015. doi:10.1038/nmat4232.

[69] E. D. Demaine, M. L. Demaine, V. Hart, G. N. Price, and T. Tachi. (non) existence of pleated folds: how paper folds between creases. *Graph. Combinator.*, 27(3):377–397, 2011. doi:10.1007/s00373-011-1025-2.

[70] J. A. Faber, A. F. Arrieta, and A. R. Studart. Bioinspired spring origami. *Science*, 359(6382):1386–1391, 2018. doi:10.1126/science.aap7753.

[71] H. Yasuda and J. Yang. Reentrant origami-based metamaterials with negative poisson's ratio and bistability. *Phys. Rev. Lett.*, 114(18): 185502, 2015. doi:10.1103/physrevlett.114.185502.

[72] M. Schenk. *Folded Shell Structures*. PhD thesis, Clare College, University of Cambridge, 2011.

[73] B. G. Chen and C. D. Santangelo. Branches of triangulated origami near the unfolded state. *Phys. Rev. X*, 8(1):011034, 2018. doi:10.1103/physrevx.8.011034.

[74] S. Waitukatis, P. Dieleman, and M. van Hecke. Non-euclidean origami (unpublished). 2018.

[75] L. Cedolin and Z. P. Bǎzant. *Stability of structures: Elastic, Inelastic, Fracture and Damage Theories*. World Scientific, 2010. doi:10.1142/9789814317047.

[76] B. G. Chen, B. Liu, A. A. Evans, J. Paulose, I. Cohen, V. Vitelli, and C. D. Santangelo. Topological mechanics of origami and kirigami. *Phys. Rev. Lett.*, 116(13):135501, 2016. doi:10.1103/physrevlett.116.135501.

[77] J. M. McCarthy and G. S. Soh. *Geometric Design of Linkages*, volume 11. Springer, 2nd edition, 2006. doi:10.1007/978-1-4419-7892-9.

[78] C. H. Chiang. On the classification of spherical four-bar linkages. *Mech. Mach. Theory*, 19(3):283–287, 1984. doi:10.1016/0094-114x(84)90061-2.

[79] F. L. Duditza and G. Dittrich. Die bedingungen für die umlauffähigkeit sphärischer viergliedriger kurbelgetriebe. *Industrie-Anzeiger*, 91(71):1687–1690, 1969. URL https://www.europeana.eu/portal/en/record/2020801/dmglib_handler_docum_2163009.html.